HHS Public Access

Author manuscript

Nat Cell Biol. Author manuscript; available in PMC 2019 March 05.

Published in final edited form as:

Nat Cell Biol. 2018 June ; 20(6): 699–709. doi:10.1038/s41556-018-0109-0.

Multi-color lineage tracing reveals clonal dynamics of squamous carcinoma evolution from initiation to metastasis

Melissa Q. Reeves[1,*], **Eve Kandyba**[1], **Sophie Harris**[1], **Reyno Del Rosario**[1], and **Allan Balmain**[1,*]

[1]Helen Diller Family Comprehensive Cancer Center, UCSF

SUMMARY

Tumor cells are subjected to evolutionary selection pressures during progression from initiation to metastasis. We analyzed the clonal evolution of squamous skin carcinomas induced by DMBA/TPA treatment using the *K5CreER-Confetti* mouse and stage-specific lineage tracing. We show that benign tumors are polyclonal, but only one population contains the *Hras* driver mutation. Benign papillomas are therefore monoclonal in origin, but recruit neighboring epithelial cells during growth. Papillomas that never progress to malignancy retain several distinct clones, whereas progression to carcinoma is associated with a clonal sweep. Newly generated clones within carcinomas demonstrate intratumoral invasion and clonal intermixing, often giving rise to metastases containing two or more distinct clones derived from the matched primary tumor. These data demonstrate that late stage tumor progression and dissemination are governed by evolutionary selection pressures that operate at a multicellular level, and thus differ from the clonal events that drive initiation and the benign-malignant transition.

INTRODUCTION

Most tumors are commonly thought to arise from the clonal expansion of a single, initiated cell[1,2], followed by generation of distinct subclones that may cooperate to drive tumor growth or progression[3,4]. Inflammation of the tissue microenvironment leading to “field cancerization” (for review see Dotto[5]) and the discovery of oncogenic point mutations in groups of cells in histologically normal tissue[6,7] have raised the possibility that multiple cells within a field can participate in the earliest stages of cancer development[8–10]. Studies using the dimethylbenzanthracene/12-O-tetradecanoylphorbol-13-acetate (DMBA/TPA) skin carcinogenesis model have also identified stem-cell-like cells driving the distinct clonal growth patterns of benign and malignant tumors[11,12]. Although metastases were once thought to be clonal outgrowths of single disseminated tumor cells, both cell biological [13–16] and genetic approaches[17,18] have provided evidence for polyclonal contributions. Here we have exploited both multi-color cellular lineage tracing[19] and next generation sequencing analysis of a mouse model which recapitulates the mutation burden and heterogeneity seen

*Corresponding author.

in human tumors[20–23] to interrogate clonal dynamics at multiple stages of tumor advancement, from initiation to metastasis.

RESULTS

The Confetti mouse contains a four-color cassette, which upon Cre-activation labels each cell with one of four fluorophores: GFP, YFP, RFP, or CFP[19]. Topical tamoxifen treatment of *K5CreER-Confetti* mouse backskin gave rise to durable (up to 18 months) labeling of skin cells with all four colors (Fig. 1A, B) with a slight bias in frequency[19] for RFP (Fig. 1C). Mice were treated with the carcinogen DMBA 10 days after their final dose of tamoxifen, to allow tamoxifen clearance[24], and subsequent twice-weekly TPA treatment [25] (Fig. 1D) generated benign papillomas beginning around 6-8 weeks.

Multiple cell populations contribute to benign papillomas

The majority of papillomas (75%) harvested at 20 weeks post-initiation showed mainly a single color (the “bulk color”) but had several, smaller populations of distinct colors also visible. These originated from the base of the tumor and formed “streaks” up the side of the papilloma (Fig. 2A), and were similar to patterns in papillomas observed in carcinogen-treated chimaeric mice[9]. However early stage papillomas harvested at 12 weeks after DMBA treatment were single-colored (Fig. 2B, C), suggesting that the streak patterns developed over time and did not make a substantive contribution to the earliest papilloma growth. Analysis of papillomas harvested between 27 and 49 weeks after DMBA treatment showed patterns identical to those observed at 20 weeks. The increase in “streaked” papillomas between 12 weeks and both later timepoints was statistically significant ($p=0.006$ and $p=0.00001$ between 12 vs. 20 weeks and 12 weeks vs. terminal papillomas respectively) (Fig. 2C). Streaks comprised on average 6% (ranging from 1% to 17%) of colored cells in the tumor in both the 20-week and terminal cohorts, (Fig. 2D). Cross-sectioning of “streaked” tumors confirmed the whole-mount pattern (Fig. 2E, Supplementary Fig. 1A, B), and H&E staining of serial sections revealed no histological differences between cells that belonged to a streak and adjacent cells that did not (Fig. 2E-H).

We monitored tumors in two cohorts of control mice (either no tamoxifen, 217 tumors, 10 mice; or no *K5CreER* cassette, 177 tumors, 7 mice) to determine whether stochastic recombination of the Confetti cassette could affect our observations. In both cohorts, we observed an extremely low level of Confetti leakiness. In a small number of papillomas—4 papillomas from the “no tamoxifen” cohort (2.3%) and 10 papillomas from the “no K5CreER” cohort (4.6%)—one or two individual spots of color were observed. These were significantly smaller in size than the “streaks” described above (<15 cells) and lacked any trends in localization. Further, no leakiness was observed in carcinomas or metastases from either cohort (0/11 and 0/9 carcinomas and 0/8 and 0/9 metastases in “no tamoxifen” and “no K5CreER” cohorts respectively).

Minor cell populations are recruited cells, and papillomas are monoclonal in origin

To address the question of whether the “streaks” that develop during papilloma growth were genetically initiated cells, four multi-colored tumors were separated by fluorescence-

activated cell sorting (FACS) (Fig. 3A, Supplementary Fig. 1C), followed by Sanger sequencing of *Hras* in "bulk" and "streak" cells from each papilloma[22,26]. We found a the expected *Hras* Q61L mutation in the bulk population of all four tumors, however, all the streak populations were wild-type for *Hras* by Sanger sequencing (Fig. 3B).

By sequencing whole exomes (Fig. 3B-H), we found that the streaks carried fewer total mutations (4.8 vs 13.3 mutations per megabase in the bulk population) (Fig. 3C). The bulk populations however carried a distinct DMBA-specific A>T mutation signature associated with mis-repair of adducts formed with adenosine residues in DNA[27] and consistent with previous sequencing of tumors from this model[22,28]. Streak populations carried almost no A>T mutations and instead had a mutation signature primarily comprised of G>T mutations (Fig. 3D), possibly due to oxidative stress induced by the tumor promoter TPA[22]. In support of this, G>T mutations in these populations showed no strand bias, consistent with being reactive oxygen species (ROS)-induced and in contrast to the carcinogen-induced A>T mutations (Fig. 3F).

Further, while the bulk population carried gains of chromosome 7, effectively duplicating the mutant copy of the *Hras* gene located on this chromosome[22,29], copy number profiles of the streak populations were completely silent (Fig. 3E). The mutation and copy number data together suggest that these streaks are derived from normal, neighboring K5+ keratinocytes (evidenced by the Confetti labeling) which were co-opted to grow and proliferate abnormally in the tumor.

Although the streak populations lacked the common *Hras* driver mutation and showed no sign of genomic instability, both bulk and streak populations alike carried potentially oncogenic mutations[30–32] (Fig. 3G, Supplementary Table 1 & 2). In the bulk populations, in addition to *Hras* mutations, we found mutations in *Trp53*, *Ep300*, *Fat1*, and *Ncor1*, all of which we have previously reported to be recurrently mutated in DMBA-induced tumors[22,28] (Fig. 3G, Supplementary Table 1). In the streak populations, we detected two *Notch* mutations, *Notch1* D545H and *Notch2* P863H (Fig. 3G, Supplementary Table 2), both of which are in N-terminal epidermal growth factor (EGF)-like repeat domains responsible for Ca2+ binding. Interestingly, *Notch* mutations in this specific region are associated with squamous tumor development[31] and have also been previously detected in DMBA-induced tumors[22,28]. Similar mutations in *Notch* have been found in histologically normal microdissected areas of human skin and have been proposed to confer a selective growth advantage[7]. We also detected a *Pten* M1R mutation, expected to result in a loss of translation of tumor suppressor *Pten*, and a stopgain mutation in *Map3k1* (G1371X), which confers an early truncation in the kinase domain. Missense mutations and deletions of *MAP3K1* are have been reported in a number of tumor types, including breast and prostate cancers[33]. These mutations together suggest that the streak populations, despite lacking an initiating *Hras* mutation, are subject to similar selection pressures as the bulk tumor.

We examined the variant allele fractions (VAF) of mutations in the bulk and streak populations to assess their respective clonalities. The average VAFs in the bulk populations were significantly higher than those in their respective streak counterparts (Fig. 3H, on average, VAF = 0.36 in bulk vs. 0.19 in streak populations, $P < 2.2 \times 10^{-16}$). This is

consistent with the bulk population being a single population containing many clonal mutations (as well as some subclonal mutations acquired during continued tumor growth), while the sorted streak populations were each comprised of multiple populations (e.g., multiple streaks of the same color; see Fig. 2A). Finally, we asked whether the presence of mono-color patches in the interfollicular epidermis at the time of initiation could have masked polyclonal contributions to the "bulk" population of these tumors. Given the relatively small patch size (average 6–7 cells in cross-section) and the large number of papillomas collected (380 papillomas), such masking was statistically improbable, as a tumor lacking an obvious "bulk" color was never observed. We further looked at the mutant allele fraction of DMBA-associated T>A mutations in the bulk population of each tumor sequenced, which are expected to have a mutant allele fraction around 0.5 in a clonal population. The mean mutant allele fraction for T>A mutations was 0.43, with a unimodal distribution, in agreement with the "bulk" color population being comprised of a single initiated clone, and potentially a small number of cells belonging to matching-colored streaks.

Non-progressing papillomas harbor multiple equipotent clones, but a single clone drives progression to malignancy

In order to investigate the cellular dynamics of malignant progression, we next activated Confetti labeling in established early papillomas. DMBA/TPA-treated *K5CreER-Confetti* mice were given 2 doses of topical tamoxifen 8 weeks after DMBA treatment, when papillomas were typically 0.5–2mm in size (Fig. 4A). This resulted in widespread labeling of papillomas with all four Confetti colors (Fig. 4B), activating fluorescence in approximately 45% of tumor cells, as well as labeling of adjacent skin.

We monitored these mice over a period of 6–7 months after labeling, to compare clonal dynamics in papillomas that never underwent malignant progression to to those that progressed. In non-progressing papillomas, typically several large mono-color clones emerged (Fig. 4C-E) and persisted through the time of sacrifice 6 months later. In these non-progressing papillomas, no significant clone intermixing occurred (Fig. 4F, G and Supplementary Fig. 2A-D), and no single dominant clone emerged within the tumor. Further, neighboring clones were histologically indistinguishable from one another (Supplementary Fig. 2A-D).

In contrast, a different pattern was seen in carcinomas that developed from papillomas in this same cohort of mice. Carcinomas, which were surgically resected when they reached 1cm in diameter, were all comprised of a single color clone (Fig. 4H, I). Approximately half (6/13) were entirely colored (3 RFP, 2 YFP, 1 CFP), while the others were entirely uncolored. Single-color patterns were confirmed by FACS for 11 of 13 tumors (remaining 2 carcinomas were not sorted) and by sectioning. To assess the significance of this, we compared this single-color pattern in carcinomas with the number of visible colored lobes in papillomas that were age-matched to a carcinoma or obtained at sacrifice. While carcinomas were comprised of only one color, papillomas contained on average 2.5 distinctly colored, externally visible lobes ($p = 0.0003$). This number is likely an underestimate, as only externally visible papilloma lobes were scored on whole-mount tumors. For example, 2 such

distinct lobes are seen in the right-hand whole-mount tumor in Fig. 4D, however cross-sectioning of this tumor shown in Fig. 4E reveals at least 3 additional lobes (e.g., small CFP lobe in lower right, small RFP lobe in the middle, and GFP lobe at top previously indistinguishable from large YFP lobe).

It should be noted that in assessing carcinoma color, we focused on the tumor core. It is common for a carcinoma to grow partially beneath the skin, and so at the periphery it is not unusual to see hair follicles and interfollicular epidermis that differ in histology as well as color pattern from the tumor (Supplementary Fig. 2E), which we excluded from analysis. Further, although the streaks observed in papillomas could be detected in these carcinomas as well as carcinomas that developed from mice in the skin-labeling experiment described above, they were restricted to the periphery of the tumor (Fig. 4J). This suggests that whatever role these genetically more “normal” streaks might play in papilloma development, they are not essential to the tumor after progression to malignancy.

We conclude that while non-progressing premalignant tumors retain distinct clones, progression to malignancy is characterized by the sweep of a single clone, which dominates in malignant carcinomas.

Intratumoral invasion and clonal intermixing is a feature of carcinoma progression

In order to investigate clonal diversity and behavior during the benign-malignant transition itself, we next labeled papillomas at 24 weeks, closer to the time of progression (Fig. 5A, B). As in the 8-week labeling experiment, papillomas which did not progress to carcinomas over the following 6 months exhibited multiple colored regions. Carcinomas that emerged in this experiment, however, showed a range of labeling patterns, falling into three categories: multi-colored, speckled, and single-colored. These patterns appeared to correlate with the latency between tamoxifen labeling and carcinoma appearance and harvest (Fig. 5C), suggesting that we were able to observe snapshots of tumor dynamics at distinct points in time during progression.

In five carcinomas harvested between 2 and 6 weeks after labeling, we observed numerous distinctly-colored clones growing side by side (Fig. 5D-G, Supplementary Fig. 3). We observed that at the intersection of colored subclones, mixing of cell populations could be seen (Fig. 5F, Supplementary Fig. 4A), and that subclones could not be distinguished from each other by H&E (Fig. 5E, G). Distinct subclones, interestingly, displayed differential proliferative capacities, evidenced by levels of Ki67 staining (Supplementary Fig. 3). Whether the more proliferative subclone(s) would eventually come to dominate the carcinoma is unclear.

In contrast to this highly multi-color pattern in carcinomas that emerged shortly after labeling, carcinomas harvested 5 to 10 weeks after tamoxifen treatment typically exhibited a single dominant color clone, but also contained “speckled” patches in which cells of a distinct color were locally intermixed with the contiguous, dominant color clone (Fig. 6A-D, Supplementary Fig. 4B). Carcinomas could have multiple such localized speckle patches of distinct colors (Fig. 6C). These speckles displayed a pattern reminiscent of the border between two clones in the multi-color carcinoma (Fig. 5F), and were indistinguishable by

H&E (Fig. 6E). Neither the speckled cells nor the speckled regions showed particular co-localization with microenvironmental structures, including lymphatic vessels (stained for with LYVE-1) or blood vessels (CD31) (Fig. 6F, G; Supplementary Fig. 5A). Squamous tumor speckles were positive for K14 (Supplementary Fig. 5B), consistent with this pattern being the result of intermixing of two tumor clones, rather than aberrant Confetti activation in a stromal or other cell type.

To address the possibility that the speckled subclones were the remnants of clones being outcompeted by the dominant clone, we quantified localized Ki67 levels in both populations. These data revealed that the speckled subclones were nearly always growing at the same rate or faster than the dominant clone with which they were locally intermixed (Fig. 6H). These observations, along with proliferation data from the multi-color tumors, rather indicate that carcinoma growth is driven by several, intermixed subclones, and further that these subclones emerge after the clonal sweep associated with progression to malignancy (Fig. 6I, J). This pattern is distinct from the equipotent clones observed in papillomas (Fig. 6I, J), which tended to remain localized to specific lobes with clear boundaries (Fig. 4E-G) rather than displaying the broad intermixing seen in carcinomas.

Metastasis can be polyclonal

Metastases in the DMBA/TPA tumor model develop after surgical resection of the primary tumor, mimicking the course of human clinical practice and making it a uniquely suitable model for interrogating the patterns of clonal evolution that take place during tumor dissemination to distant sites. For mice in all Confetti labeling cohorts, primary carcinomas were surgically removed when they reached 1cm in diameter, enabling prolonged survival of the animals and subsequent harvesting of any metastases that developed. On average, mice received their first surgery 32 weeks after DMBA treatment (range: 26-43 weeks), and survived an additional 6 weeks (range: 2-16 weeks). We collected a total of 40 metastases from 14 mice labeled at either of the two earlier timepoints (e.g., labeling of pre-initiation skin or 8-week papillomas), and these were uniformly single-colored (Fig. 7A, B), consistent with the clonal patterns in carcinomas in these mice. Further, in the majority of mice (9/12, 75%) in which multiple metastases were collected, metastases to distinct locations were the same color as one another, with as many as 8 matching-colored metastases found in one mouse (Fig. 7A, B). This is in agreement with previously published phylogenetic trees from this model demonstrating that most commonly, all metastases arise from the same primary tumor[22]. This prior work[23] suggested that metastatic dissemination occurs before surgical resection of the primary tumour, and in some cases at relatively early stages of tumor development, as shown by the existence of many “private” mutations that are unshared between primary carcinomas and their matched metastases. Our data showing that metastases from animals with early Confetti activation are invariably comprised of one single color could either mean that metastasis is a clonal event, or that polyclonal dissemination took place after an early clonal sweep, followed by generation of distinct genetic subclones of the same color.

To address these possible scenarios, we investigated the clonality of the metastases in mice in which Confetti labeling occurred at 24 weeks—the only cohort bearing multi-color

primary carcinomas. We collected 12 metastases from 5 mice, and observed metastases comprised of multiple distinctly-colored cellular populations in 3 of the 5 mice (Fig. 7C). While this cohort was small, the finding of multi-colored metastases in 3 mice (60%) was significant compared to 0/14 mice (0%) in the earlier cohorts ($p = 0.010$, Fisher's exact test). In one case, we observed 3 multi-color metastases in the same animal, with two lymph node metastastases and a lung metastasis all comprised of a mix of RFP and YFP cells (Fig. 7C).

For two additional cases of multi-color metastases, we used exome sequencing to ask whether the distinct cell populations in each metastasis were from the same primary tumor. The first case we sequenced was a lymph node metastasis in which K14+ cells (i.e., tumor cells) were 75% uncolored and 25% GFP+, and intermixed in a speckling pattern (Fig. 7D). The lymph node metastasis shared 350 mutations with one of three primary carcinomas in the mouse (Carcinoma A) (Fig. 7E, F). We could not initially be certain whether these 350 mutations were present in both the uncolored and GFP+ cells in the metastasis, so we asked whether mutations in the other carcinomas (Carcinoma B and Carcinoma C, Fig. 7E) were present at low levels in the metastasis, particularly in loci well-covered by sequencing reads (>50×), and found they were not. We also examined mutations in the metastasis that were not shared with Carcinoma A for contributions from an unidentified primary tumor, which would have contributed its own fingerprint of DMBA-induced T>A signature mutations[22]—however, we found only 4 T>A mutations in the metastasis that were not present in Carcinoma A. We conclude that no evidence exists in the sequencing data that would support the possibility that the uncolored cells and GFP+ cells in this metastasis originated from different primary tumors but rather, both cell populations arose from Carcinoma A.

Interestingly, Carcinoma A was a predominantly uncolored tumor with a significant GFP+ speckle region, visible in the middle and right of the tumor cross section (Fig. 7F). Both the uncolored cells and GFP+ cells in this region were highly proliferative (Fig. 7G, H, 62% and 56% Ki67+ respectively). This carcinoma also contained YFP+ and RFP+ speckle regions, visible at the left side of the cross section (Fig. 7F). However despite the presence of these YFP+ and RFP+ cells in the primary tumor, apparently only the GFP+ and uncolored populations contributed to metastasis.

We performed exome sequencing on a second case of multi-color metastasis, a lymph node metastasis from another mouse which contained both RFP+ and uncolored K14+ tumor cells (Supplementary Fig. 6A). In this case, we sorted the RFP+ and uncolored populations by FACS (Supplementary Fig. 6B), sequenced, and again confirmed that they originated from the same primary tumor on the basis of shared mutations and shared copy number alterations (Supplementary Fig. 6C).

We conclude that metastases, in contrast to the earlier stages of tumor progression, do not arise from a single cell within the primary tumor that has acquired metastatic properties, but rather that multiple cells within progressed lesions have the capacity to disseminate and seed at distant sites. These data therefore agree with a polyclonal model of metastatic dissemination. Notably, the distinct clones seen in metastases showed the pattern of intimate intermixing (Fig. 7D) that was a feature of progression to carcinoma.

DISCUSSION

We have exploited multi-color lineage tracing using the Confetti mouse to investigate the clonal dynamics that govern each stage of tumor progression from initiation to metastasis. Others had previously used mouse models to demonstrate that papillomas were possibly polyclonal in origin[9], or that DMBA-initiated papillomas can contain cells that do not harbor the known initiating *HrasQ61L* mutation[10]. Our data demonstrate that these cells were not co-initiators of the papilloma, as they lacked the genetic changes, including the initiating *Hras* mutation, trisomy of chromosome 7 and DMBA mutation signature, that are characteristic of papillomas. This implies that the presence of multiple cellular populations in the tumor is not in itself evidence of true polyclonal initiation, although it has historically been interpreted as such in studies of both mouse models and human tumors[34,35]. The streaks we observed were reminiscent of a similar radial streaking pattern displayed by lineage-tracing of Krt15+ hair follicle bulge stem cells during wound healing[36], calling to mind the analogy of a tumor to a wound that never heals[37]. However, their presence appears to not be necessary for progression to carcinoma, as they become increasingly marginalized during malignant conversion. Interestingly, Krt15-positive stem cells also make only a transient contribution to normal healing wounds[36,38].

Labeling of established papillomas at 8 or 24 weeks after initiation allowed us to detect distinct patterns of clonal evolution during progression to malignancy. Papillomas that had not progressed after 6 months consisted of 2-4 distinct colored clones (Fig. 6I) which could have arisen from rare papilloma stem cells[11,12]. However, progression to carcinoma occurred after a clonal sweep resulting in the emergence of one dominant clone. Labeling papillomas at 24 weeks showed that most carcinomas that emerged within the next 10 weeks contained two or more intermixed, proliferating cellular populations (Fig. 6J), that may represent functionally distinct cells that cooperate, through paracrine or juxtacrine interactions[3,4]. Similar processes may contribute to tumor dissemination, as multiple carcinoma clones frequently participated in metastasis. Such clonal cooperativity has been observed in small-cell lung cancer cell lines in vitro and in vivo[3], and in a model of MMTV (mouse mammary tumor virus)-driven breast cancer[4], and even during bacterial evolution over thousands of generations in culture[39]. Given the importance of cellular and genetic heterogeneity in human cancer prognosis[40], further studies of this symbiosis may foster development of new approaches to inhibit these interactions for cancer therapy.

METHODS

Mice and carcinogenesis.

To induce tumors, male and female K5CreER-Confetti FVB/N mice were shaved and treated with 25mg DMBA dissolved in 200μL acetone either 10 days after final dose of tamoxifen (skin activation experiment) or at 8 weeks of age (tumor activation experiments). Mice subsequently received TPA (200μL of a 10^{-4} M solution in acetone) twice a week for 20 weeks, following established chemical carcinogenesis protocol[25]. Carcinomas were surgically resected when they reached a size of >1 cm in longest diameter, and mice given 0.24mL meloxicam (Boehringer Ingelheim, 5mg/mL solution) for recovery. Mice were sacrificed when disease progressed, per animal care requirements. At sacrifice, papillomas

and carcinomas were removed from skin, and all internal tumors were resected. All animal experiments were approved by the University of California San Francisco Laboratory Animal Resource Center (protocol approval #AN159869). This work complies with all relevant ethical regulations regarding animal research.

Confetti labeling.

Tamoxifen (Sigma) was dissolved overnight in sunflower seed oil at a concentration of 10mg/mL. Mice were treated with 400μL (4mg) per dose, applied to the back skin topically, and were shaved the day prior to first treatment. For skin activation experiment, mice were given 4 doses every other day for a total of 16mg. For tumor activation experiments, mice were given 2 doses for a total of 8mg, spaced 2 days apart, at either 8 or 24 weeks.

Tissue harvesting.

Skin, tumor, and metastatic tissues harvested for sectioning were kept at 4°C in 10% formalin overnight, in a gradient of 15% / 20% / 30% sucrose on the second day, in 30% sucrose overnight the second night, and then embedded in OCT (Tissue-Tek, Sakura) and stored at −80°C until sectioning.

Digestion for FACS.

For tumors that were FACS sorted, a piece of the tumor was first removed for embedding in OCT and imaging. For carcinomas, skin tissue along the edge of the carcinoma was also removed. Tumors were then finely chopped, washed with PBS, digested in 4mg/mL Collagenase A (Sigma-Aldrich) for 1 hour at 37°C, and then resuspended in 0.25% Trypsin-EDTA (Gibco Life Technologies) and incubated on a shaker at 37°C for 1 hour. Trypsin was neutralized with an equal volume of FBS, and digested tumor filtered through a 40μm filter, pelleted, and resuspended in FACS buffer (2% FBS) for sorting.

Quantification of Confetti labeling.

To quantify Confetti activation in the skin, a strip of skin oriented along the spine was collected for 5 mice 10 days after the final dose of tamoxifen, e.g., the day that DMBA treatment would have begun. To quantify Confetti activation in tumors, papillomas were surgically removed 3 days after the final dose of tamoxifen. Tissues were harvested and embedded in OCT as described above, and 5μm sections were taken for quantification. For each sample, a minimum of 10 images were taken at 40× with a 6D Nikon microscope, and nuclei and colored cells of each color were manually counted in ImageJ.

Quantification of multi-color papillomas.

At sacrifice, back skin was removed intact from mouse and imaged whole on an MVX10 fluorescent stereoscope, which could distinguish RFP, CFP, and YFP/GFP. YFP and GFP were not distinguishable from each other under this microscope. Tumors on each back skin were counted, and color(s) recorded. For statistical calculations (e.g., Figure 2C), mice which had fewer than 3 papillomas were excluded as they did not provide sufficient data (this led to the exclusion of 2 mice).

Quantification of streak populations.

To calculate the percent of colored cells comprised by streak populations, number of sorted RFP, CFP, and YFP/GFP cells were used. Due to weakness of the CFP fluorophore, bulk-CFP tumors (CFP confirmed by sectioning) were widely variable as to the number of CFP+ cells that could be collected; to reduce the large amount of noise introduced by this, we used only bulk-RFP, bulk-YFP, and bulk-GFP tumors for these calculations.

Nucleic acid extraction.

DNA was extracted from tumors using Qiagen DNeasy Blood & Tissue Kit, following manufacturer's instructions. In cases where DNA was extracted after FACS sorting, protocol was modified as follows to improve yield: (1) After sorting, FACS collection tube was spun down at 3,000rpm for 10 minutes and cells resuspended in 200μL PBS before initial lysis step; (2) Wash step with buffer AW2 was done twice. DNA concentration and quality were determined by Nanodrop spectrophotometry.

Sanger sequencing of *Hras* locus.

Hras locus containing codon 61 was PCR amplified using primer pair AAGCCTGTTGTTTTGCAGGA (forward) and GGTGGCTCACCTGTACTGATG (reverse). PCR product was purified using Exonuclease I (USB) and Shrimp Alkaline Phosphatase (Affymetrix), and Sanger sequencing was performed using the forward primer listed above by MCLAB. Images were taken using FinchTV.

Exome sequencing.

DNA samples were submitted to Otogenetics Corporation (Atlanta, GA) for mouse exome capture and sequencing. Illumina libraries were made from qualified fragmented gDNA using SPRIworks HT Reagent Kit (Beckman Coulter) and the resulting libraries were subjected to exome enrichment using SureSelectXT Mouse All Exon (Agilent) following manufacturer's instructions. Enriched libraries were tested for enrichment by qPCR and for size distribution and concentration by an Agilent Bioanalyzer 2100. The samples were then sequenced on an Illumina HiSeq2500 using Rapid v2 SBS chemistry which generated paired-end reads of 106 nucleotides.

Sequence alignment, processing and quality control.

Reads were mapped to the GRCm38/mm10 version of the *Mus musculus* genome using BWA (version 0.7.12)[41] with default parameters. The Picard MarkDuplicates module was used to remove duplicates from the data (version 1.131; http://broadinstitute.github.io/picard). The Genome Analysis Tool Kit (GATK-Lite) toolkit (version 2.3-9)[42] module IndelRealigner and BaseRecalibrator were used to preprocess the alignments. During base quality recalibration, dbSNP variants were used as known sites, according to GATK Best Practices recommendations[43]. Finally, alignment and coverage metrics were collected using Picard. We sequenced an average of 42 million unique reads per sample. Targeted bases were sequenced to a mean depth of 50, and more than 75% of targeted bases were sequenced to 20× coverage or greater.

Variant calling.

SNVs were called using somatic variant detection program MuTect (version 1.1.7)[44]. Each tumor was called against its matched normal tissue (tail), and calls were filtered against a database of known *Mus musculus* germline SNPs available at ftp.ncbi.nih.gov/snp/organisms/mouse_10090/VCF/genotype, as well as against a panel of normal tails from this experiment. Results were further filtered to calls with a minimum read depth of 10 at the locus for both tumor and matched normal, and to calls where at least one alternate read had a mapping quality score of 60 or higher. Variants were annotated using Annovar (downloaded on 2/4/2016)[45], and these annotations were used as the basis for assessing exonic variants as synonymous, nonsynonymous, stopgain, or stoploss. Mutations in cancer-associated genes were identified, where cancer-associated genes were considered to be those commonly mutated in head and neck squamous cell carcinoma[31] or cutaneous skin squamous cell carcinoma[32] in The Cancer Genoma Atlas data, or on a previously published list of cancer driver genes[30].

Copy number calling was done with CNVkit[46], and tumor copy number status was called against a panel of normal tails from the same sequencing batch.

Mutation context.

For mutation spectrum analysis, SNVs in all tumors were annotated with 1 of 96 possible trinucleotide context substitutions (6 types of substitutions × 4 possible flanking 5'-bases × 4 possible flanking 3'-bases), using MuTect output, and counts of each mutation context were summed.

Phylogenies.

To build phylogenetic trees, absolute distance matrices were calculated based on the presence of mutations in the sample, based on filtered MuTect calls. Rooted trees were built with use of the Analyses of Phylogenetics and Evolution (APE) package and manhattan calculation method implemented in R version 2.15. Relationships between metastases and primary tumors were determined on the basis of shared mutations.

Quantification of colored lobes in papillomas labeled at 8 weeks.

Papillomas were imaged whole on an MVX10 fluorescent stereoscope. Images were taken to record observations, and these whole-tumor images were used to count the number of distinctly-colored lobes on each tumor. It was possible to identify RFP, CFP, YFP/GFP, and uncolored lobes, however YFP and GFP could not be distinguished from each other using this microscope. Selected tumors from this cohort were also embedded in OCT as described above, sectioned, and 5μm sections were imaged with a Nikon 6D scope to confirm lobe quantifications done with the whole-mount tumor. Results from imaging these sections correlated well with whole-mount observations. For statistical analysis, in comparing number of colored lobes in papillomas and carcinomas, we excluded fully-uncolored papillomas and carcinomas because it is impossible to distinguish a monoclonal tumor from a poorly-labeled polyclonal tumor with multiple uncolored subclones; thus, we included only tumors where at least one Confetti color was visible in the analysis.

Classification of labeling pattern in tumors labeled at 24 weeks.

For carcinomas harvested in 24 week labeling experiment, all carcinomas were embedded in OCT as described above, sectioned, and imaged with a Nikon 6D microscope in order to classify their labeling pattern. At least two distinct pieces of each carcinoma were used, and at least 3 serial sections taken 100μm or more apart. Tumors classified as multi-color contained large, contiguous patches of at least 2 of the 4 Confetti colors. Tumors classified as speckled showed one or more “speckle” populations of cells that were a distinct color from the surrounding tumor cells, and which formed localized patches of non-contiguous cells (in contrast to contiguous patches observed in “multi-color” tumors), and which could be identified in at least 3 serial sections from the tumor. Tumors classified as single-color contained only one color population of cells in the tumor, excluding hair follicles and interfollicular epidermis that was sometimes present at the edge of the tumor.

Immunofluorescent staining.

Slides with 5μm tumor sections were brought to room temperature, post-fixed in 4% paraformaldehyde for 8 minutes, and washed in PBS for 5 minutes. For Ki67 staining, slides were blocked in 5% goat serum/0.3% Triton-X100 for 1 hour. Ki67 antibody (Cell Signaling #9129) was used at a concentration of 1:300 in 2% goat serum/0.3% Triton-X100 and left on slides overnight. Slides were washed 3× in PBS, and incubated with goat anti-rabbit Alexa Fluor 647 (Thermofisher #A21246) secondary antibody at a concentration of 1:200 for 90 minutes, and then washed 2× with PBD (PBS with 0.1% Tween-20) followed by PBS. For K14, LYVE-1, and CD31 staining, slides were blocked in 10% donkey serum/0.1% Triton-X100 for 15 minutes. K14 antibody (Biolegend #905301) was used at a concentration of 1:2000, and allowed to incubate on slides for 2 hours. For lymphatic vessel staining, LYVE-1 antibody (Abcam #ab14917) was used at the concentration of 1:100, and allowed to incubate on slides for 2 hours. For blood vessel staining, CD31 antibody (Abcam #ab28364) was used at a concentration of 1:300, and allowed to incubate on slides for 2 hours. For K14, LYVE-1 and CD31 staining, secondary antibody of either donkey anti-rabbit Alexa Fluor 594 (Thermofisher, A21207) or Alexa Fluor 488 (Thermofisher #A21206) was selected to avoid interference with Confetti colors in relevant samples, and slides were incubated with secondary antibody at a concentration of 1:500 for 1 hour and washed 3× with PBS.

Quantification of Ki67.

Tumor sections stained for Ki67 were imaged with a Nikon 6D microscope. Quantification was based on manual counts using ImageJ of at least 3 images taken at 40× magnification, where individual cells could be identified and classified based on both presence or absence of Ki67 and Confetti labeling color.

Statistics and reproducibility.

Statistics and P-values throughout the manuscript were calculated with Student’s two-tailed t-test, using R (version 3.2.3). For Fig. 2c, 2d, 3h, 5c, 5m, and 6g, two-sample t-tests were performed to calculate difference between two distributions as shown. For Fig. 3f one-sample t-test was performed for each sample to evaluate null hypothesis of mean equal to 0.5 (i.e., even distribution of mutation between strands). Skin labeling experiment was

performed in 8 mice for 12-week observation, 4 mice for 20-week observation, and 9 mice for observation of terminal disease, with reproducible results between all mice in each cohort. 8-week labeling experiment was performed in 4 mice, divided into 2 cohorts, with reproducible results between all mice. 24-week labeling experiment was performed in 5 mice, divided into 3 cohorts, with reproducible results between all mice.

Data availability

Exome sequence data that support the findings of this study have been deposited in the European Nucleotide Archive under accession number ERP107810. Source data for Fig. 1c, 2c, 2d, 3c, 3d, 3f, 5c, 6h, and 7g have been provided as Supplementary Table 3. All other data supporting the findings of this study are available from the corresponding author on reasonable request.

Supplementary Material

Refer to Web version on PubMed Central for supplementary material.

ACKNOWLEDGEMENTS

This work was supported by US National Cancer Institute (NCI) grants RO1CA184510, UO1 CA176287, and R35CA210018 and the Barbara Bass Bakar Professorship of Cancer Genetics. M.Q.R. is supported by NCI F31 NRSA award CA206459. We are greatly appreciative of help and comments from our colleagues in refining this study and manuscript, and would also like to thank T. Nystul and R. Akhurst for providing the Confetti mouse, S. Vlachos and D. Laird for assistance with whole-mount fluorescent imaging, D. Larsen and the Nikon Imaging Center for microscopy training and making the Nikon 6D microscope available, and to S. Elmes and the Laboratory for Cell Analysis core for flow cytometry training.

REFERENCES

1. Nowell PC The clonal evolution of tumor cell populations. Science 194, 23–8 (1976). [PubMed: 959840]
2. Greaves M & Maley CC Clonal evolution in cancer. Nature 481, 306–313 (2012). [PubMed: 22258609]
3. Calbo J et al. A Functional Role for Tumor Cell Heterogeneity in a Mouse Model of Small Cell Lung Cancer. Cancer Cell 19, 244–56 (2011). [PubMed: 21316603]
4. Cleary AS, Leonard TL, Gestl S. a & Gunther EJ Tumour cell heterogeneity maintained by cooperating subclones in Wnt-driven mammary cancers. Nature 508, 113–7 (2014). [PubMed: 24695311]
5. Dotto GP Multifocal epithelial tumors and field cancerization: Stroma as a primary determinant. J. Clin. Invest 124, 1446–53 (2014). [PubMed: 24691479]
6. Jonason AS et al. Frequent clones of p53-mutated keratinocytes in normal human skin. Proc. Natl. Acad. Sci. U. S. A 93, 14025–14029 (1996). [PubMed: 8943054]
7. Martincorena I et al. High burden and pervasive positive selection of somatic mutations in normal human skin. Science 348, 880–6 (2015). [PubMed: 25999502]
8. Reddy AL & Fialkow PJ Influence of dose of initiator on two-stage skin carcinogenesis in BALB/c mice with cellular mosaicism. Carcinogenesis 9, 751–754 (1988). [PubMed: 3130203]
9. Winton DJ, Blount MA & Ponder BA Polyclonal origin of mouse skin papillomas. Br. J. Cancer 60, 59–63 (1989). [PubMed: 2803917]
10. Li S et al. A keratin 15 containing stem cell population from the hair follicle contributes to squamous papilloma development in the mouse. Mol. Carcinog 52, 751–9 (2013). [PubMed: 22431489]

11. Driessens G, Beck B, Caauwe A, Simons BD & Blanpain C Defining the mode of tumour growth by clonal analysis. Nature 488, 527–31 (2012). [PubMed: 22854777]
12. Huang PY et al. Leucine-rich G-protein coupled receptor 6 (Lgr6) is a cancer stem cell marker in mouse squamous carcinomas. Nat. Genet In Press
13. Harney AS et al. Real-Time Imaging Reveals Local, Transient Vascular Permeability, and Tumor Cell Intravasation Stimulated by TIE2hi Macrophage-Derived VEGFA. Cancer Discov 5, 932–43 (2015). [PubMed: 26269515]
14. Cheung KJ, Gabrielson E, Werb Z & Ewald AJ Collective invasion in breast cancer requires a conserved Basal epithelial program. Cell 155, 1639–51 (2013). [PubMed: 24332913]
15. Aceto N et al. Circulating Tumor Cell Clusters Are Oligoclonal Precursors of Breast Cancer Metastasis. Cell 158, 1110–1122 (2014). [PubMed: 25171411]
16. Maddipati R & Stanger BZ Pancreatic Cancer Metastases Harbor Evidence of Polyclonality. (2015). doi:10.1158/2159-8290.CD-15-0120
17. Gundem G et al. The evolutionary history of lethal metastatic prostate cancer. Nature 520, 353–7 (2015). [PubMed: 25830880]
18. Sanborn JZ et al. Phylogenetic analyses of melanoma reveal complex patterns of metastatic dissemination. Proc. Natl. Acad. Sci 112, 10995–11000 (2015). [PubMed: 26286987]
19. Snippert HJ et al. Intestinal Crypt Homeostasis Results from Neutral Competition between Symmetrically Dividing Lgr5 Stem Cells. Cell 143, 134–144 (2010). [PubMed: 20887898]
20. Swanton C Intratumor Heterogeneity: Evolution through Space and Time. Cancer Res 72, 4875–4882 (2012). [PubMed: 23002210]
21. Westcott PMK et al. The mutational landscapes of genetic and chemical models of Kras-driven lung cancer. Nature 517, 489–492 (2014). [PubMed: 25363767]
22. McCreery MQ et al. Evolution of metastasis revealed by mutational landscapes of chemically induced skin cancers. Nat. Med 21, 1514–1520 (2015). [PubMed: 26523969]
23. McFadden DG et al. Genetic and clonal dissection of murine small cell lung carcinoma progression by genome sequencing. Cell 156, 1298–311 (2014). [PubMed: 24630729]
24. Schepers AG et al. Lineage tracing reveals Lgr5+ stem cell activity in mouse intestinal adenomas. Science 337, 730–5 (2012). [PubMed: 22855427]
25. Wong CE et al. Inflammation and Hras signaling control epithelial-mesenchymal transition during skin tumor progression. Genes Dev 27, 670–82 (2013). [PubMed: 23512660]
26. Quintanilla M, Brown K, Ramsden M & Balmain A Carcinogen-specific mutation and amplification of Ha-ras during mouse skin carcinogenesis. Nature 322, 78–80 (1986). [PubMed: 3014349]
27. Bigger CA, Sawicki JT, Blake DM, Raymond LG & Dipple A Products of binding of 7,12-dimethylbenz(a)anthracene to DNA in mouse skin. Cancer Res 43, 5647–51 (1983). [PubMed: 6315214]
28. Nassar D, Latil M, Boeckx B, Lambrechts D & Blanpain C Genomic landscape of carcinogen-induced and genetically induced mouse skin squamous cell carcinoma. Nat. Med 21, (2015).
29. Aldaz C, Trono D, Larcher F, Slaga T & Conti C Sequential trisomization of chromosomes 6 and 7 in mouse skin premalignant lesions. Mol. Carcinog 2, 22–6 (1989). [PubMed: 2499343]
30. Vogelstein B et al. Cancer Genome Landscapes. Science 339, 1546–58 (2013). [PubMed: 23539594]
31. Stransky N et al. The mutational landscape of head and neck squamous cell carcinoma. Science 333, 1157–60 (2011). [PubMed: 21798893]
32. Pickering CR et al. Mutational landscape of aggressive cutaneous squamous cell carcinoma. Clin. Cancer Res 20, 6582–92 (2014). [PubMed: 25303977]
33. Pham TT, Angus SP & Johnson GL MAP3K1: Genomic Alterations in Cancer and Function in Promoting Cell Survival or Apoptosis. Genes and Cancer 4, 419–26 (2013). [PubMed: 24386504]
34. Novelli MR et al. Polyclonal origin of colonic adenomas in an XO/XY patient with FAP. Science 272, 1187–90 (1996). [PubMed: 8638166]
35. Parsons BL Many different tumor types have polyclonal tumor origin: Evidence and implications. Mutat. Res 659, 232–247 (2008). [PubMed: 18614394]

36. Ito M et al. Stem cells in the hair follicle bulge contribute to wound repair but not to homeostasis of the epidermis. Nat. Med 11, 1351–1354 (2005). [PubMed: 16288281]

37. Dvorak HF Tumors: wounds that do not heal. Similarities between tumor stroma generation and wound healing. N. Engl. J. Med 315, 1650–9 (1986). [PubMed: 3537791]

38. Plikus MV et al. Epithelial stem cells and implications for wound repair. Semin. Cell Dev. Biol 23, 946–53 (2012). [PubMed: 23085626]

39. Good BH, McDonald MJ, Barrick JE, Lenski RE & Desai MM The dynamics of molecular evolution over 60,000 generations. Nature 551, 45–50 (2017). [PubMed: 29045390]

40. McGranahan N & Swanton C Biological and Therapeutic Impact of Intratumor Heterogeneity in Cancer Evolution. Cancer Cell 27, 15–26 (2015). [PubMed: 25584892]

41. Li H & Durbin R Fast and accurate short read alignment with Burrows-Wheeler transform. Bioinformatics 25, 1754–60 (2009). [PubMed: 19451168]

42. McKenna A et al. The Genome Analysis Toolkit : A MapReduce framework for analyzing next-generation DNA sequencing data. Genome Res 20, 1297–1303 (2010). [PubMed: 20644199]

43. DePristo M. a et al. A framework for variation discovery and genotyping using next-generation DNA sequencing data. Nat. Genet 43, 491–8 (2011). [PubMed: 21478889]

44. Cibulskis K et al. Sensitive detection of somatic point mutations in impure and heterogeneous cancer samples. Nat. Biotechnol 31, 213–9 (2013). [PubMed: 23396013]

45. Wang K, Li M & Hakonarson H ANNOVAR: functional annotation of genetic variants from high-throughput sequencing data. Nucleic Acids Res 38, e164 (2010). [PubMed: 20601685]

46. Talevich E, Shain AH & Bastian BC CNVkit: Copy number detection and viziualization for targeted sequencing using off-target reads. (2014). doi:10.1101/010876

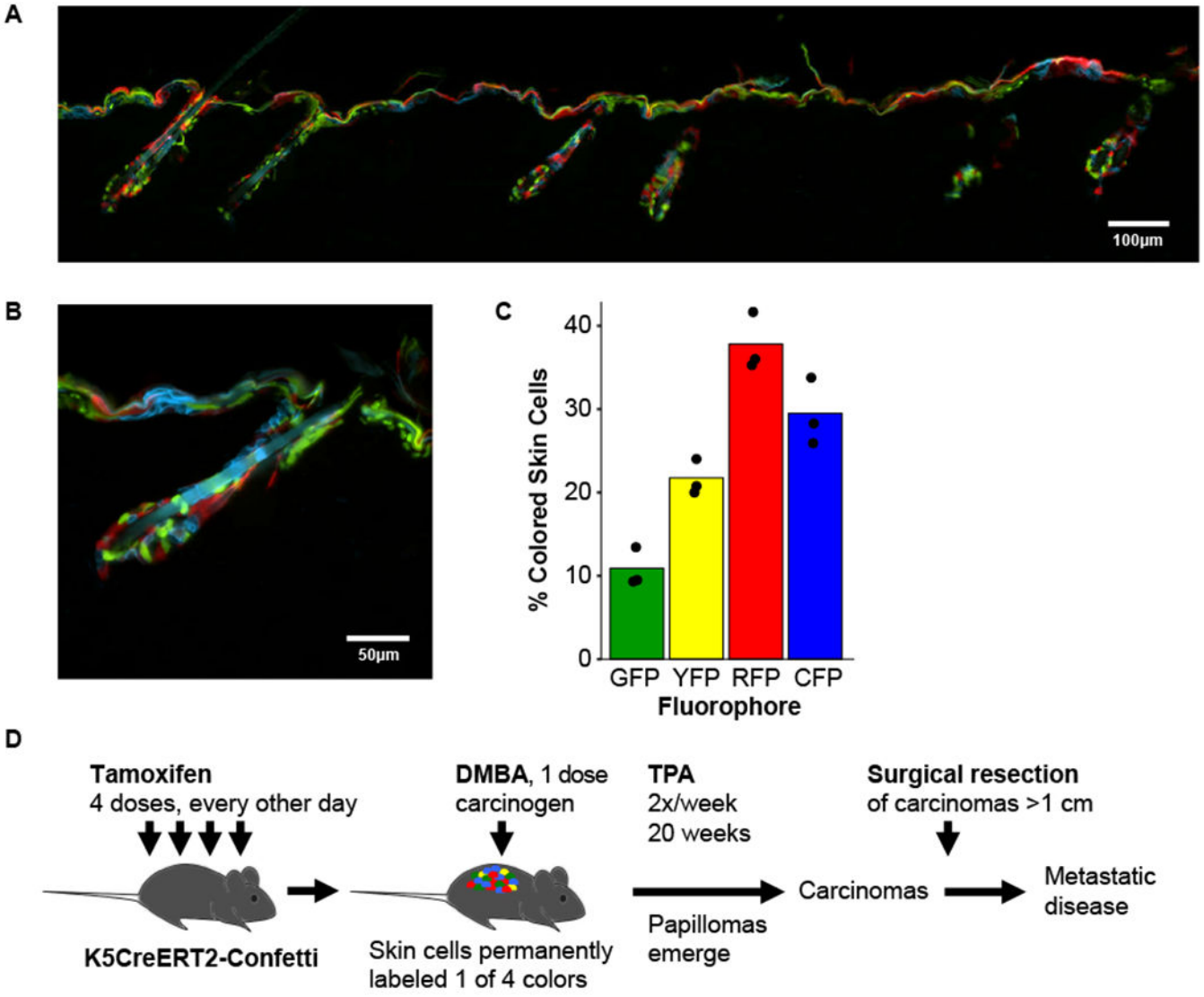

Figure 1. Tamoxifen-induced Confetti labeling of the skin.

(A and B) Back skin sections of K5CreER-Confetti mice (5 mice), treated with 4 doses of tamoxifen to activate Confetti recombination. Sections taken 10 days after final dose of tamoxifen, at 10× (A) and 40× (B) magnification.

(C) Proportion of labeled skin cells in back skin expressing each Confetti fluorophore, 10 days after final dose of tamoxifen (n=3 mice, 44 panels). See Supplementary Table 3 for statistics source data.

(D) Schematic of tumorigenesis strategy. K5CreER-Confetti mice are treated with 4 doses of tamoxifen to activate Confetti labeling, and then treated with the carcinogen DMBA 10 days after final tamoxifen dose, followed by biweekly treatments with tumor promoter TPA. Dozens of benign papillomas emerge beginning at 6-8 weeks, a subset of which progress to carcinomas. Carcinomas are surgically resected when they reach 1cm in diameter, and mice go on to develop metastatic disease.

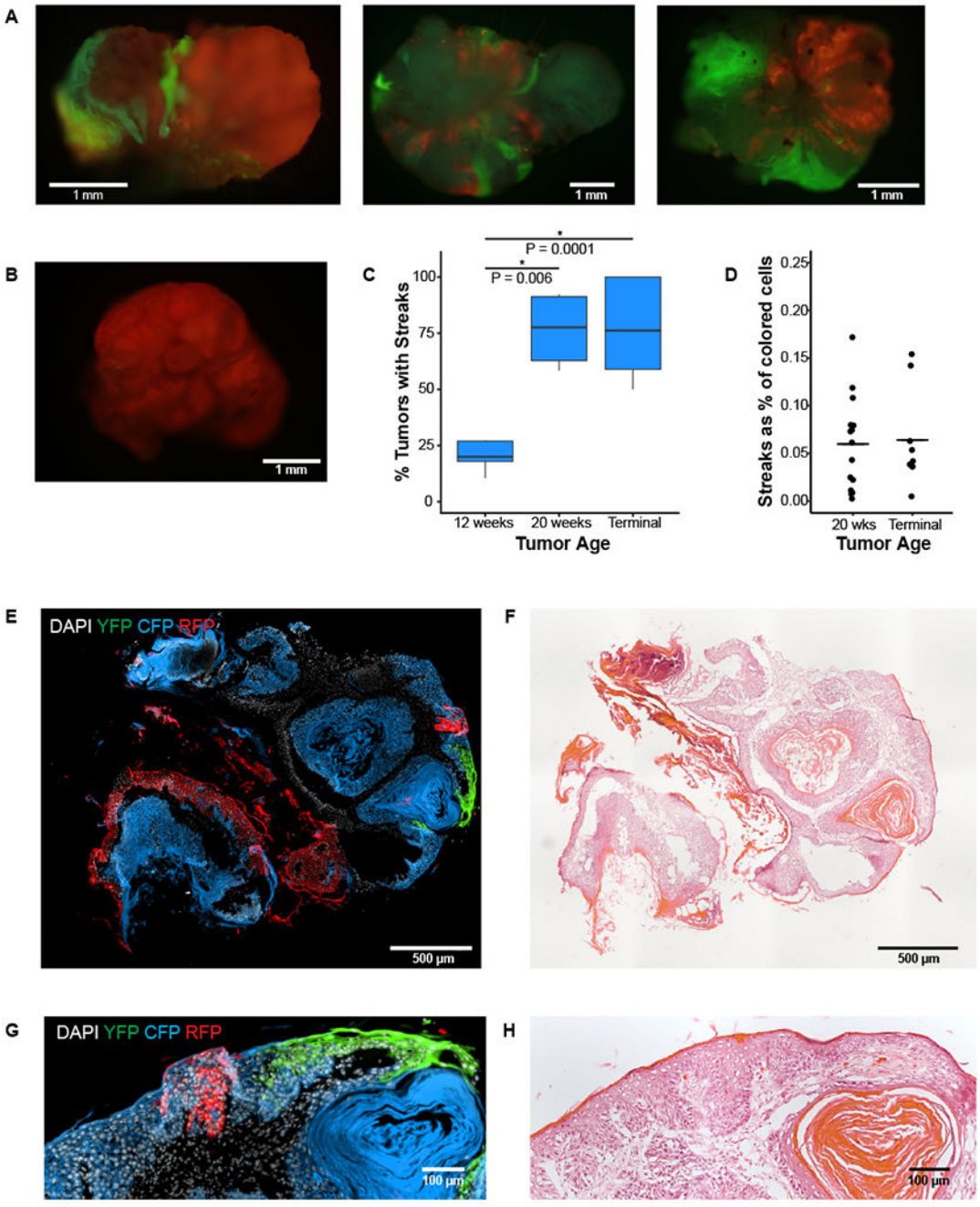

Figure 2. Streaked appearance of papillomas arising from Confetti-labeled skin.

(A) Whole papillomas with multi-color streaking pattern, characteristic of 20-week papillomas (77 tumors), viewed from a fluorescent dissecting microscope. Left panel views the papilloma from the side, center and right panels view papillomas from the bottom.

(B) Whole papilloma lacking streaking pattern, characteristic of 12-week papillomas (222 tumors), viewed from a fluorescent dissecting microscope from the side.

(C) Percentage of papillomas in each mouse that exhibited a multi-color pattern, organized by time point at which papillomas were harvested. Data based on 222 12-week tumors (n=8

mice), 77 20-week tumors (n=4 mice), and 81 terminally benign tumors (n=9 mice). Box plots show boxes extending from first to third quartile, with median marked by a cross bar. Asterisk (*) indicates $P < 0.05$, two-sided Student's t-test.

(D) Streak cells as a percentage of colored cells in a multi-color papilloma. Data based on n=15 twenty-week and n=9 terminal FACS-sorted tumors. Cross-bar shows mean in each cohort.

(E) Cross-section of a multi-color, streaked papilloma, characteristic of 20-week and terminal papillomas (77 and 81 tumors respectively). The bulk of the papilloma is CFP+, and RFP+ and YFP+ streaks are visible. Nuclei are marked with DAPI.

(F) H&E of adjacent section of papilloma shown in panel (E).

(G) Close up of RFP+ and YFP+ streaks in CFP+ papilloma at 40× magnification. Nuclei are marked with DAPI.

(H) H&E of adjacent section of papilloma region shown in panel (G). Cell belonging to bulk CFP+ and to streak RFP+ and YFP+ populations are pathologically indistinguishable. See Supplementary Table 3 for statistics source data.

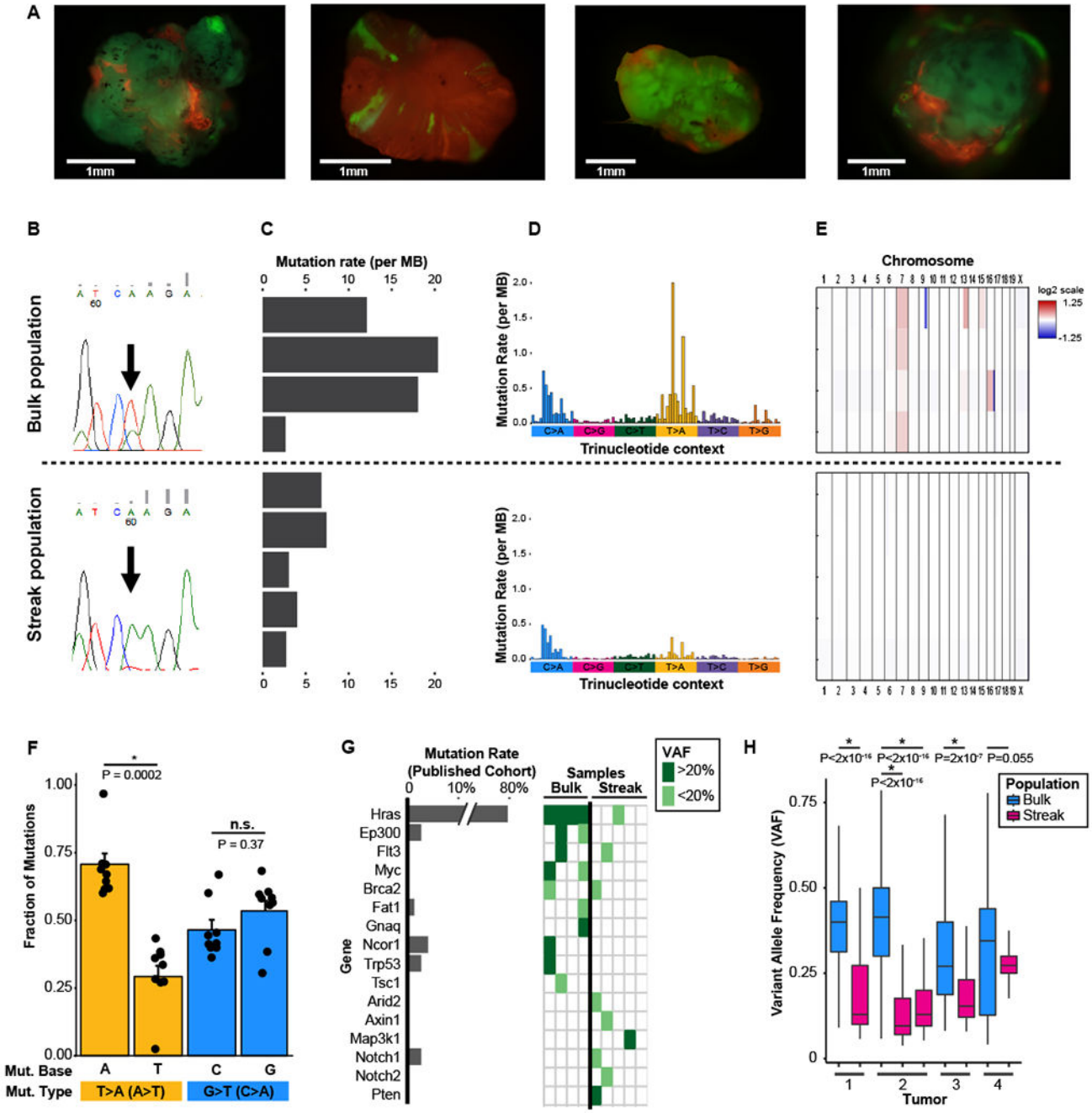

Figure 3. Genetic analysis of bulk and streak papilloma populations.

(A) Whole-tumor fluorescent dissecting scope images of the 4 multi-color papillomas separated for sequencing of “bulk” and “streak” populations.

(B) Sanger sequencing of *Hras* in bulk (top) and streak (bottom) population in a multi-color tumor (n = 4 tumors). Arrow shows chr7:141192550; when mutated to T this results in an *Hras* Q61L mutation.

(C) Mutation rate per megabase, based on exome sequencing to 50×, of 4 bulk, 5 streak populations.

(D) Trinucleotide context of mutations in 4 bulk, 5 streak populations. X-axis denotes 96 possible trinucleotide contexts, grouped by base pair change. T>A mutations (yellow) are frequent in bulk population but near-absent in streak populations. C>A(G>T) mutations are observed in both populations.

(E) Copy number alterations. Chromosomes arranged along X-axis; samples arranged on Y-axis in same order as panel (C). Gains of chromosome 7, on which *Hras* is located, observed in all 4 bulk populations; no copy number alterations are observed in streak populations.

(F) Frequency of each base on the coding strand being mutated for T>A(A>T) (yellow) and G>T(C>A) (blue) mutations (n = 9 samples). T>A(A>T) mutations showed a bias for "A" on the coding strand at the mutated site; G>T(C>A) mutations showed no bias. Bar graphs show mean±s.e.

(G) Comparison of cancer-associated mutations in bulk and streak samples (right, each column represents one sample) with frequency of mutation in these genes in a previously published cohort[23] (right). Variant allele frequency (VAF) color-coded dark green for mutations present in >20% of reads, and light green for <20%. Note that although a mutation in *Hras* was detected in a single streak sample, it was present at a low allele fraction.

(H) VAFs of mutations in bulk and streak samples (n = 573, 181, 932, 322, 339, 107, 135, 845, 56 mutations, left to right). Samples organized by tumor of origin; in each case VAFs in the bulk population are higher consistent with a population of clonal origin. Box plots extend first to third quartile; median marked by crossbar; P-values based on two-sided Student's t-test. Supplementary Table 3 for source data.

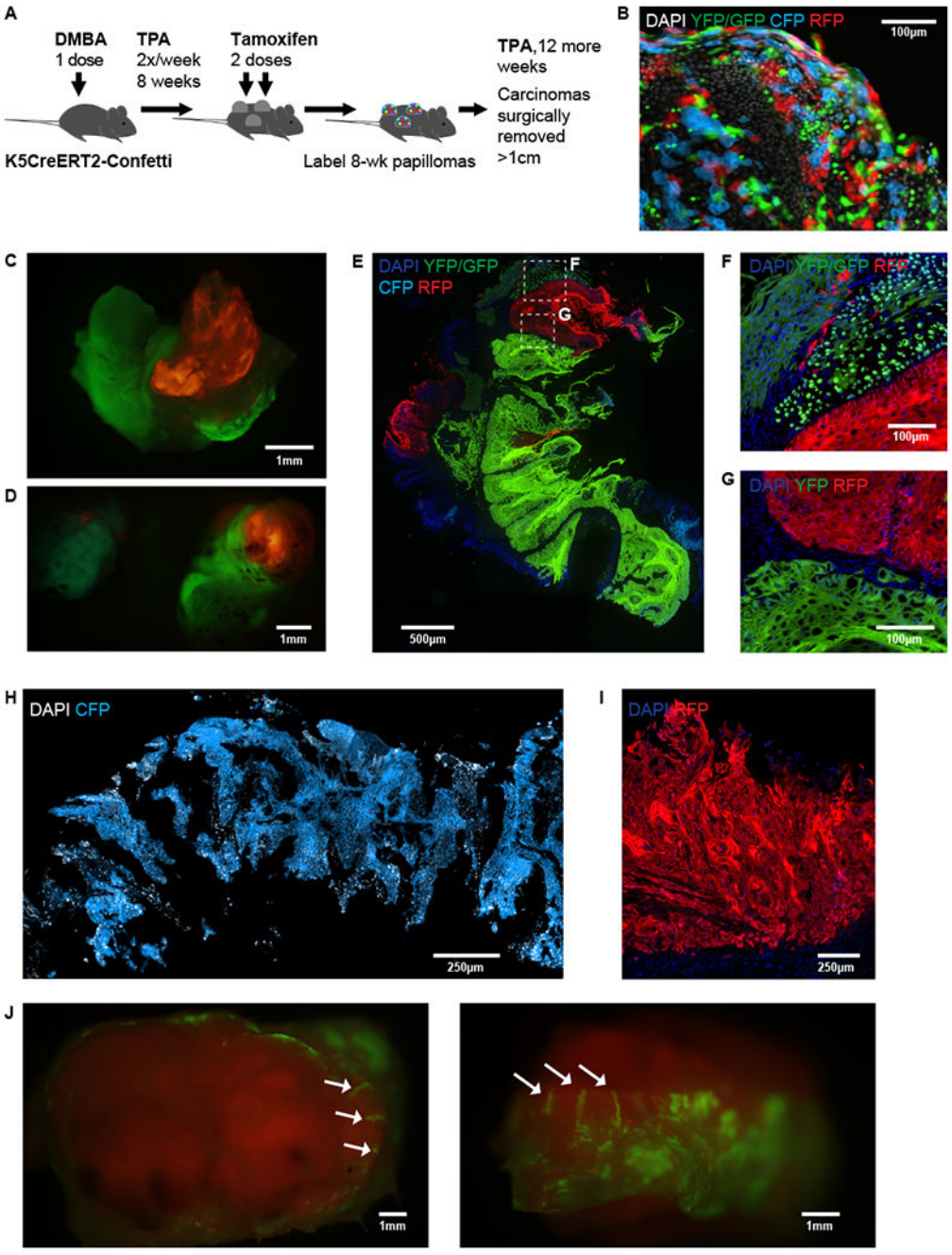

Figure 4. Tumor evolution following Confetti labeling at 8 weeks.

(A) Schematic of experimental design. DMBA/TPA-induced papillomas were allowed to grow for 8 weeks in K5CreER-Confetti mice. Confetti labeling was subsequently activated 8 weeks after DMBA treatment with 2 doses of tamoxifen, and TPA treatment was continued. (B) Cross-section of a papilloma labeled at 8 weeks post-DMBA, 3 days after final dose of tamoxifen, exhibiting Confetti labeling (3-day labeling verification based on 3 tumors). (C, D) Whole papillomas labeled at 8 weeks post-DMBA (25 papillomas), viewed from with side with a fluorescent dissecting microscope. Images taken 8 weeks (D) and 27 weeks (C)

after tamoxifen. Green and red lobes are visible in (C) and right-hand tumor in (D), blue lobe and small red lobe are visible in left-hand tumor in (D).

(E) Cross-section of right-hand tumor in (D), a papilloma labeled at 8 weeks post-DMBA. Image taken 8 weeks after tamoxifen. Nuclei are marked with DAPI.

(F and G) High magnification images of tumor shown in (E), highlighting boundaries between colored lobes where limited intermixing is seen. Nuclei are marked with DAPI.

(H and I) Cross-sections of carcinomas from mice in which Confetti labeling was activated 8 weeks post-DMBA, each exhibiting only a single color (13 carcinomas). Nuclei are marked with DAPI.

(J) Whole carcinoma from a mouse treated with tamoxifen at 8 weeks (13 carcinomas), viewed from the top (left) and side (right). Streaks, indicated by arrows, are visible but confined to the periphery.

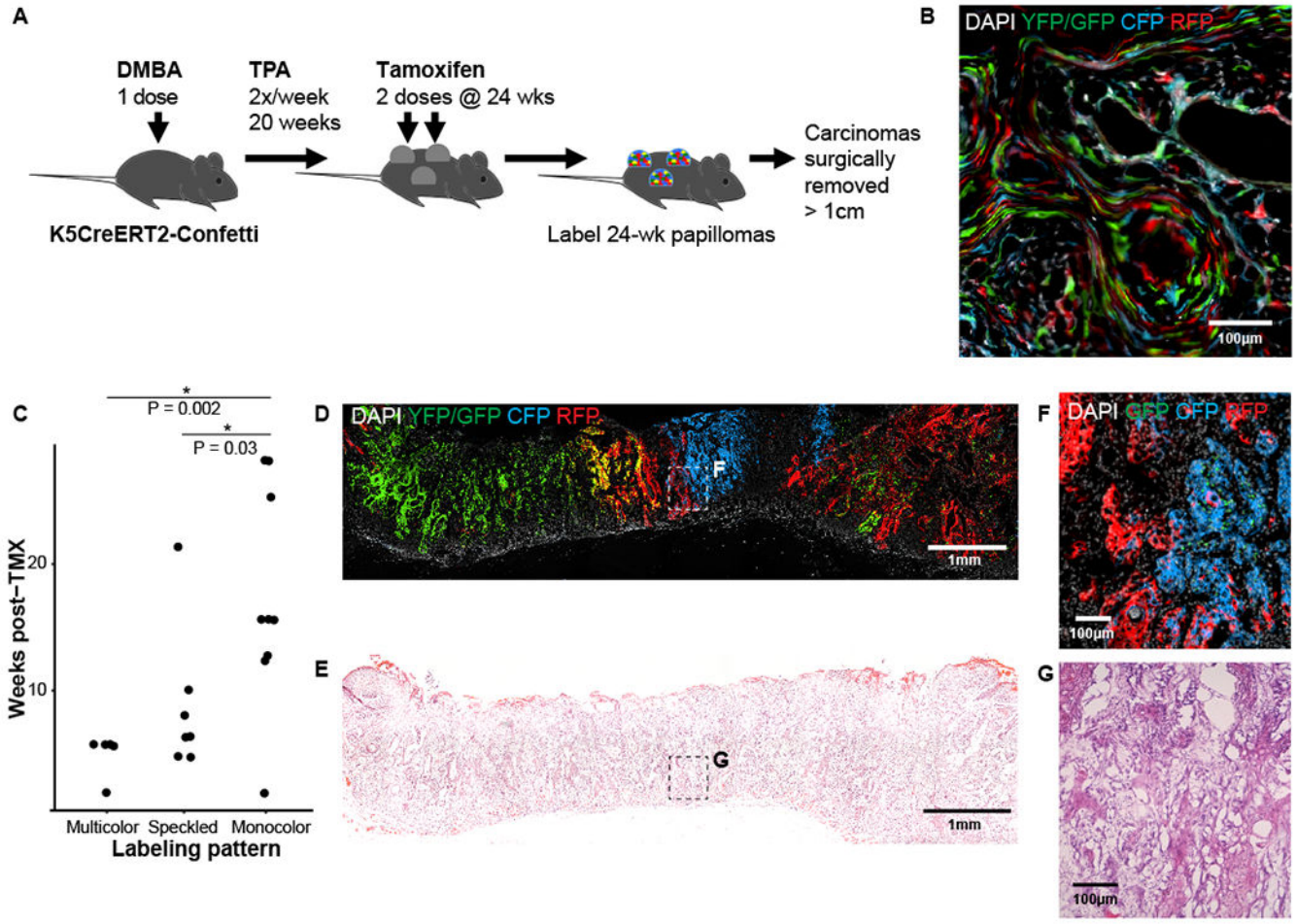

Figure 5. Carcinoma evolution following Confetti labeling at 24 weeks.

(A) Schematic of experimental design. DMBA/TPA-induced papillomas were allowed to grow for 24 weeks in K5CreER-Confetti mice. Confetti labeling was subsequently activated with 2 doses of tamoxifen.

(B) Cross-section of a papilloma labeled at 24 weeks post-DMBA, 3 days after final dose of tamoxifen, exhibiting Confetti labeling (3-day labeling verification based on 2 tumors).

(C) Relationship between labeling pattern observed in harvested carcinomas and the time elapsed between tamoxifen labeling and harvest. Carcinomas harvested close to time of labeling were frequently multi-color ($n = 5$), carcinomas harvested at an intermediate time point were frequently speckled ($n = 7$), and carcinomas harvested long after labeling were typically single colored ($n = 9$). Asterisk (*) indicates $P < 0.05$, two-sided Student's t-test. See Supplementary Table 3 for statistics source data.

(D) Cross-section of a multi-color carcinoma exhibiting patches of all Confetti colors.

(E) H&E of adjacent section of carcinoma shown in panel (D).

(F) Magnified region of multi-color carcinoma shown in panel (D), showing intermixing of colored cells at a boundary between RFP, CFP, and GFP clones.

(G) H&E of adjacent section of carcinoma region shown in panel (F). Cells belonging to CFP+, RFP+ and GFP+ clones are indistinguishable by H&E.

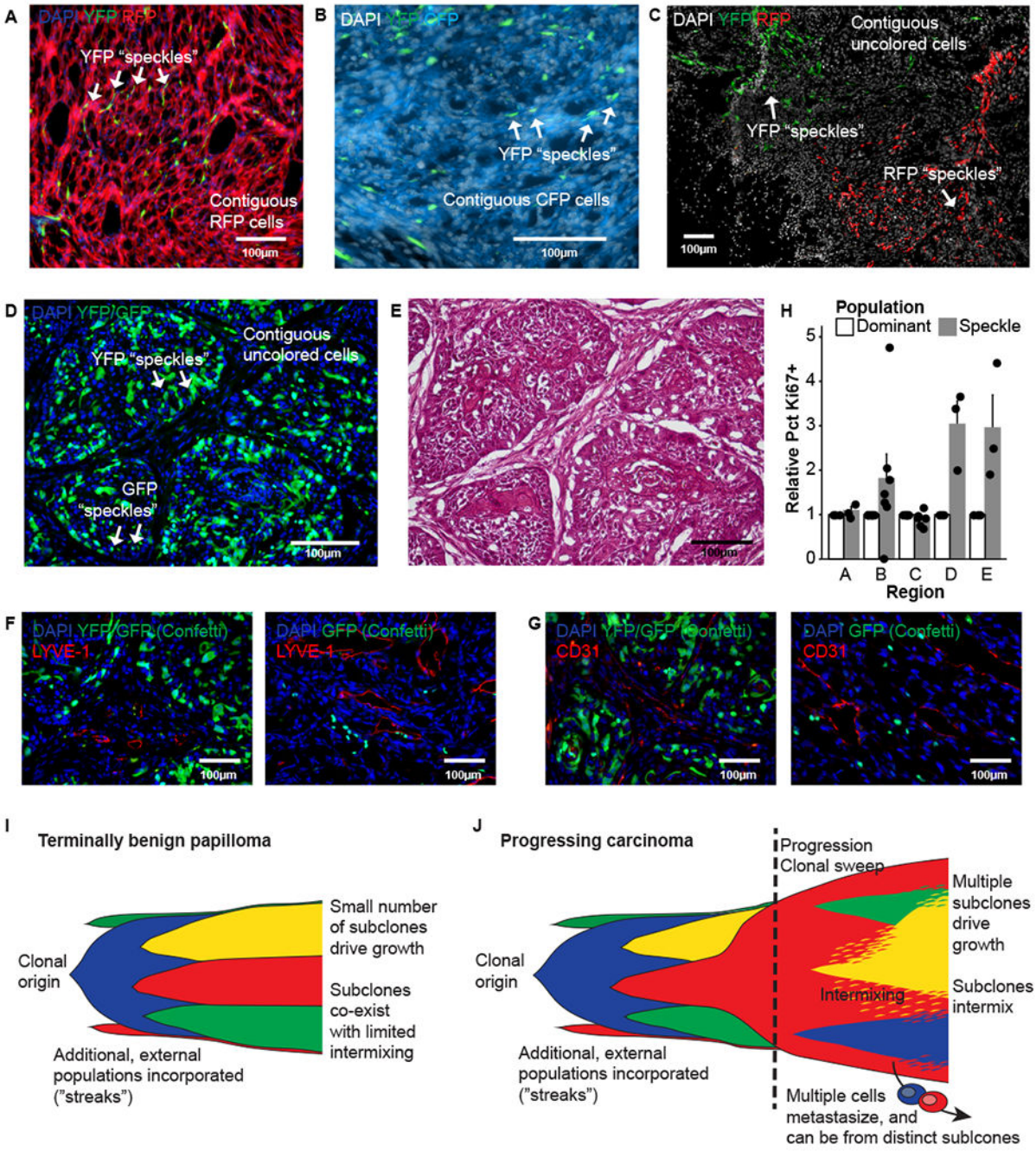

Figure 6. Speckle populations observed in carcinomas.

(A, B) Examples of colored carcinomas containing colored "speckles." RFP-dominant carcinoma with YFP speckles (A) and CFP-dominant carcinoma with YFP speckles (B). Example "speckle" cells indicated with arrows.

(C) Carcinoma containing multiple patches of differently-colored speckles. 3 of 7 speckled carcinomas displayed multiple differently-colored speckle patches. Carcinoma shown is dominated by uncolored cells (nuclei marked with DAPI), and contains YFP and RFP speckles, each localizing to distinct regions (arrows).

(D) High magnification image of a dominant-uncolored carcinoma containing YFP+ and GFP+ speckles.
(E) H&E of adjacent section of carcinoma region shown in panel (D). Cells belonging to uncolored, YFP+ and GFP+ clones are indistinguishable by H&E.
(F, G) Speckled carcinomas stained for LYVE-1 (F) and CD31 (G) (4 tumors stained, 5 sections each). No trends in localization are observed between speckles and blood vessels (CD31) or lymphatic vessels (LYVE-1).
(H) Relative levels of Ki67+ staining between dominant and speckle populations in selected local regions, representing tumors from multiple mice (counts based n = 6, 3, 6, 3, 3 sections for tumors, left to right). Bar graphs show mean±s.e. See Supplementary Table 3 for statistics source data.

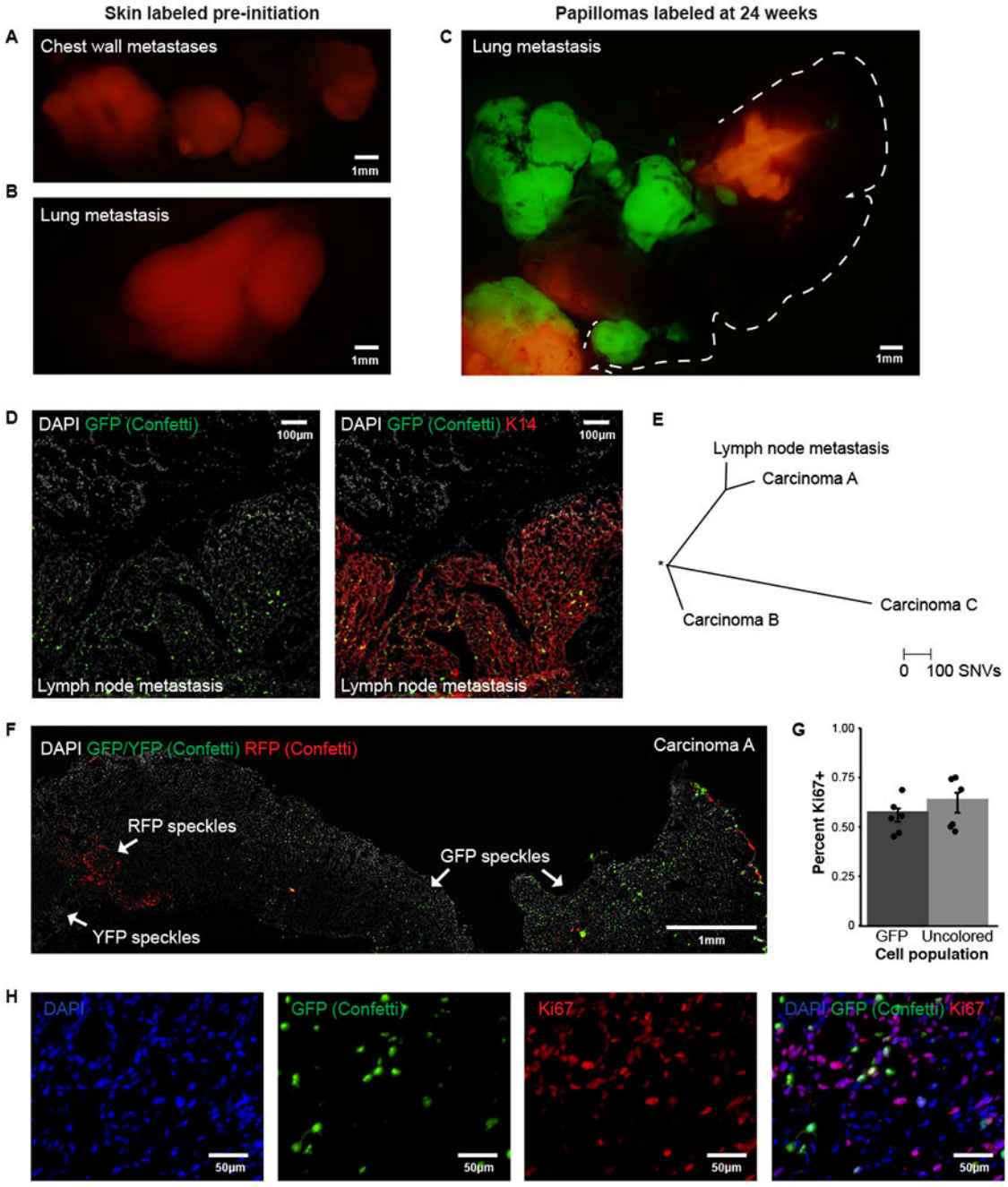

Figure 7. Evidence for polyclonal seeding of metastasis.

(A and B) Metastases to the chest wall (A) and lung (B) from a mouse in which skin was labeled pre-initiation (experimental design described in Fig. 1D, 10 mice), viewed from a fluorescent dissecting microscope. All metastases are from the same mouse, and are uniformly red (RFP+). The same pattern was observed in mice in which papillomas were labeled at 8 weeks (4 mice).

(C) Lung metastasis from a mouse in which papillomas were labeled at 24 weeks (experimental design described in Fig. 5A, 5 mice), viewed from a fluorescent dissecting

microscope, containing both red (RFP+) and green (YFP+) cells. Lung is outlined with a dashed line.

(D) Cross-section of a lymph node metastasis from a second mouse in which papillomas were labeled at 24 weeks (experimental design described in Fig. 5A, 5 mice), exhibiting a dominant uncolored cell population and GFP+ speckles (left). K14 staining of the same panel (right) demonstrates both uncolored and GFP+ cells are K14+ tumor cells.

(E) Phylogenetic tree showing relationship between all tumors in mouse bearing lymph node in panel (D). Carcinoma A (shown in panel (F)) and the lymph node metastasis share 350 mutations. Mutations and phylogenetic tree based on exome sequencing performed to a target depth of 50× for the four tumors shown (Carcinoma A, B, and C and the lymph node metastasis).

(F) Cross-section of sequence-matched Carcinoma A that gave rise to lymph node metastasis in panel (D). Carcinoma contains YFP, RFP, and GFP speckle patches indicated with arrows.

(G) Quantification of Ki67 staining of GFP+ and uncolored cells in the GFP speckle region in Carcinoma A, showing similar Ki67 levels in both populations. Staining and quantification was done in the region adjacent to right-most arrow in panel (F) ($n = 6$ sections). Bar graphs show mean±s.e. See Supplementary Table 3 for statistics source data.

(H) Illustrative Ki67 staining of GFP speckle region, quantified in panel (G).